

Article

Hot Corrosion Behavior of Co-Al-W Superalloys with Si Additions

Pengjie Zhou ^{*}, Yingjie Wang, Qilong Liu, Yanxin Qiao  and Shujin Chen

School of Materials Science and Engineering, Jiangsu University of Science and Technology, Zhenjiang 212003, China; wangyingjie1997@126.com (Y.W.); liuqilong1998@126.com (Q.L.); yxqiao@just.edu.cn (Y.Q.); chenshujin7120@126.com (S.C.)

* Correspondence: zhoupengjie@just.edu.cn

Abstract: The hot corrosion behavior of Co-9Al-9.5W-xSi (where $x = 0\%, 0.1\%, 0.5\%$, at.%) alloys in a salt mixture at 900°C was investigated. The effect of Si on hot corrosion resistance was examined using corrosion kinetics. The surface morphology of the corrosion products was explored via SEM with EDS and the phase constituents were examined using XRD. The results revealed that hot corrosion occurred as a combination of both sulfidation and oxidation behavior. With the increase in Si content, the hot corrosion resistance of the alloy was capable of remarkable advancement. Corrosion scales on the three Co-based alloys were mostly comprised of Co_3O_4 , CoO , CoAl_2O_4 , CoWO_4 , and Al_2O_3 . The hot corrosion mechanism for the Co-based alloy in the presence of 75 wt.% Na_2SO_4 and 25 wt.% NaCl deposits were analyzed.

Keywords: Co-Al-W alloys; hot corrosion; hot corrosion mechanism

1. Introduction

Superalloys are a sort of metallic material which presents superior mechanical properties and thermal stability at elevated temperatures. They also possess good thermal corrosion resistance and fatigue resistance [1,2]. Hence, they are key materials in the manufacture of aero-engines, gas turbines electricity generators, steam turbines, and petrochemical components [3–5]. These alloys are usually based on Fe, Ni, and Co, which are stable not only at room temperature but also at elevated temperatures. Ni-based superalloys are widely applied in turbine blades, primarily because of their prominent ability to withstand high-temperature creep and fatigue, but also because their cost and availability are advantageous.

However, Co-based superalloys exhibit increasing prominence based on the following factors: their superior hot corrosion resistance, flatter stress-rupture/time parameter curves, and the relatively higher melting temperature of Co compared to Ni. However, due to the lack of a stable A_3B type hardening phase, the traditional Co-based superalloy shows an inferior strength compared with Ni-based alloys. Sato et al. provided a pathway for a novel Co-based superalloy by reporting the relatively stable $\text{L1}_2\text{-Co}_3$ (Al, W) phase in the Co-Al-W system. The superiority of traditional Co-based superalloys with regard to hot corrosion resistance most likely stems from the following reasons: high-level Cr content or low diffusion coefficient of S in the Co matrix. A large number of studies examined the hot corrosion properties of this newly developed alloy [6–8] and put forward a universal mechanism for high-temperature hot corrosion [9]. When compared against Ni-based superalloys, Co-based superalloys have excellent corrosion resistance, cobalt's melting point is higher than that of nickel, and its service temperature is expected to exceed that of Ni-based superalloys [10]. Our results indicate that the Co-Al-W alloy has a higher incipient melting temperature as well as matchable mechanical properties [11–13]. Thus, this new type of γ' precipitation-strengthened Co-Al-W superalloy was found to receive increasing attention. Kazuya claimed that the γ' solvus temperature of Co-Ni-Al-W



Citation: Zhou, P.; Wang, Y.; Liu, Q.; Qiao, Y.; Chen, S. Hot Corrosion Behavior of Co-Al-W Superalloys with Si Additions. *Coatings* **2023**, *13*, 1031. <https://doi.org/10.3390/coatings13061031>

Academic Editor: Paweł Nowak

Received: 28 April 2023

Revised: 26 May 2023

Accepted: 29 May 2023

Published: 1 June 2023



Copyright: © 2023 by the authors. Licensee MDPI, Basel, Switzerland. This article is an open access article distributed under the terms and conditions of the Creative Commons Attribution (CC BY) license (<https://creativecommons.org/licenses/by/4.0/>).

quaternary alloys is high when compared with Co–Al–W ternary alloys [14]. The γ' – γ two-phase regions in the Co–Ni–Al–W–Cr system can be extended with the addition of Ni [15].

As oxidation and hot corrosion are important factors in the length of superalloy service life, it is critical to investigate the oxidation and corrosion behaviors and the way they may be affected by alloying elements [16–18]. Hot corrosion is facilitated when fabricated components work in corrosive environments, such as exposure to SO₂. Thus, hot corrosion is actually accelerated oxidation which is influenced by deposited salts [19]. When salt is placed at a higher temperature above its melting point, the oxide scales, such as Al₂O₃, Cr₂O₃, and SiO₂, may be damaged by the molten salt mixture deposited on the coating surface, causing the spallation or dissolution of the oxide scales [19,20].

Numerous efforts were made to improve mechanical strength at high temperatures and to achieve better oxidation and hot corrosion resistance [21–25]. Gao found that the hot corrosion resistance of Co–Ni–Al–W–Cr alloys varied with variations in Ni content. Increasing the content of Ni resulted in the generation of more Ni₃S₂ and the aggravation of corrosion. Nevertheless, Ni can also lead to the formation of a protective layer of Al₂O₃, which can help protect the alloys [26]. Yan discovered that oxidation resistance could be slightly reduced by the addition of Ni [24]. Xu found that Ta and Nb raised the corrosion rate of Co-based superalloys because the severe segregation of Ta and Nb is prone to hot corrosion cracks [27]. Klein illustrated that Ta and Nb degrade the oxidation resistance of Co–Al–W–B alloy, while adding Cr and Si is beneficial to the oxidation resistance of the alloy [28]. Klein also claimed that Co–Ni-based alloys with 9 and 18 at.% Ni possessed similar oxidation resistance [3].

Up to now, few studies were conducted to investigate the hot corrosion properties of Co–Al–W-based alloys. The influence of Si content on this behavior was not systematically investigated. Two ways are often adopted to improve the hot corrosion behaviors of components working at elevated temperatures. The first way is to form a dense oxide scale which can provide a satisfying protective oxide. The addition of Si, an approach to adding alloying elements, is beneficial to developing a continuous compact oxide. The other way is to introduce a coating, such as MCrAlY and Al. If the Si-bearing alloy still cannot adopt an excellent resistance to heat corrosion, a coating is then necessary. Hence, the isothermal hot corrosion behavior of Co–Al–W superalloys with varied Si contents was examined in a mixture of 75% Na₂SO₄ + 25% NaCl (wt.%) molten salt at 900 °C, and the hot corrosion mechanism was explored.

2. Materials and Methods

High purity Co (99.9 wt.%), Al (99.9 wt.%), W (99.95 wt.%), and Si (99.99 wt.%) were employed to formulate the cast ingots of Co–9Al–9.5W–xSi, where x = 0, 0.1, 0.5, in at.%. The experimental alloys were melted by vacuum arc melting. Each ingot weighed about 80 g. The chamber was evacuated to 0.1 Pa and was, subsequently, filled with a high-purity argon atmosphere. This process was repeated before melting. The alloys were repeatedly melted 6 times to obtain a homogenous polycrystalline ingot. The nominal compositions of the alloys and actual compositions are listed in Table 1. The actual compositions were investigated by EDS analysis.

Table 1. Nominal compositions and actual composition of experimental alloys (at.%).

Heat	Nominal Composition (at.%)				Actual Compo Composition (at.%)			
	Co	Al	W	Si	Co	Al	W	Si
A	Bal	9	9.5	0	81.77	8.91	9.32	-
B	Bal	9	9.5	0.1	81.87	8.85	9.28	-
C	Bal	9	9.5	0.5	81.59	8.81	9.27	0.33

The ingots were sealed in vacuum quartz capsules and then solution-treated at 1230 °C for 8 h. Subsequent aging treatment was conducted at 900 °C for 72 h. Later, the samples were quickly quenched into ice water. Specimens with dimensions of 10 × 10 × 2 mm were cut from the ingots by a conventional wire electrode cutting. The microstructures of the alloys after heat treatment are given in Figure 1. The alloys showed a similar microstructure, which was primarily composed of γ and γ' dual structures, as well as minor Co_3W presented at the grain boundary. The specimens were polished down to 600-grit SiC paper, degreased in acetone, ultrasonically cleaned in ethanol, and then dried in the air prior to slat deposition.

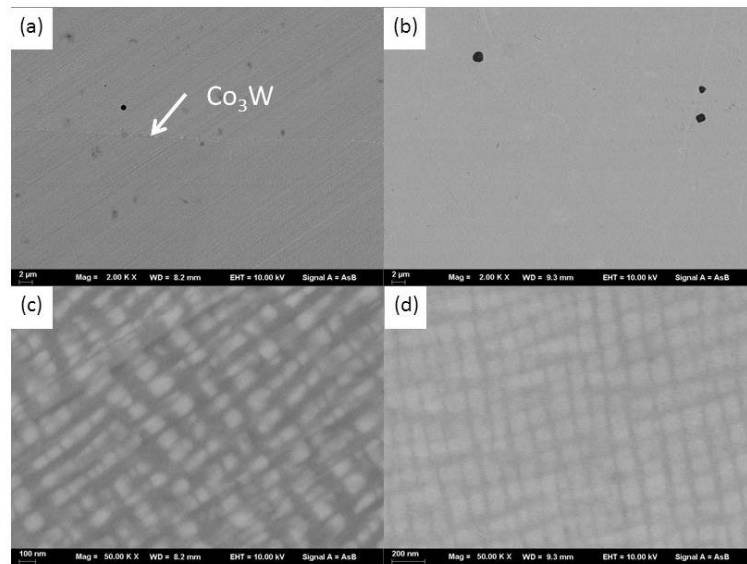


Figure 1. Microstructure of each alloy after heat treatment: (a,c) Si-Free alloy; (b,d) 0.5 Si alloy.

We performed the hot corrosion test at 900 °C in static air. Before exposure, the samples were preheated on a heating table, followed by deposition with a saturated solution of 75% Na_2SO_4 + 25% NaCl (wt.%). The amount of deposition was controlled to $2.0 \pm 0.2 \text{ mg/cm}^2$. When the furnace reached a stable target temperature, the crucibles with samples were placed in the furnace. Hot corrosion tests were conducted at 900 °C at 2, 4, 8, 16, 32, and 64 h, respectively. Corrosion kinetics was measured by thermogravimetry. The weights of the specimens before and after corrosion tests were measured by an electro balance with a precision of 0.1 mg. The crystalline phases in the hot corrosion layers were determined by using X-ray diffraction (XRD-6000, Shimadzu, Kyoto, Japan) at a scanning speed of 4 °/min. A scanning electron microscope (Merlin Compact, Zeiss, Jena, Germany) was used to examine the surface morphologies of the specimens. An attached Energy Dispersive X-ray Spectroscopy (X-Max50, Oxford Instruments Inc., Abingdon, UK) was employed to determine the chemical composition of the phases and elemental distribution of the cross-section of the samples.

3. Results

3.1. Hot Corrosion Kinetics

Figure 2 reveals the corrosion kinetics of different Co-Al-W-xSi-based superalloys with a predeposition of 75 wt.% Na_2SO_4 + 25 wt.% NaCl at 900 °C, which is the mass gain per surface area of the samples as a function of the exposure time. As shown in Figure 2, the mass gain of all samples increased with the exposure time extension. The weight gain of tested samples increased as the exposure time extended up to 64 h. After 64 h of hot corrosion, the mass gains were 64.96 mg/cm^2 , 33.91 mg/cm^2 , and 37.19 mg/cm^2 , respectively. Thus, the molten mixture of 75 wt.% Na_2SO_4 + 25 wt.% NaCl quickened the corrosion rate of the three alloys. After 8 h, the corrosion rate of alloy A was about 1.5 times

higher than that of alloy B and alloy C. Severe oxidation emerged during the testing process of specimen A. The corrosion products spalled with ease because of the stress deriving from the scale growth. Alloy A (0 Si) presents the highest mass gain of the three alloys. However, alloys B and C demonstrated a relatively slight rise in weight gain, which indicates that the use of Si can substantially enhance the hot corrosion resistance of Co-Al-W superalloys. A significant improvement can be seen in the 0.5 Si alloy.

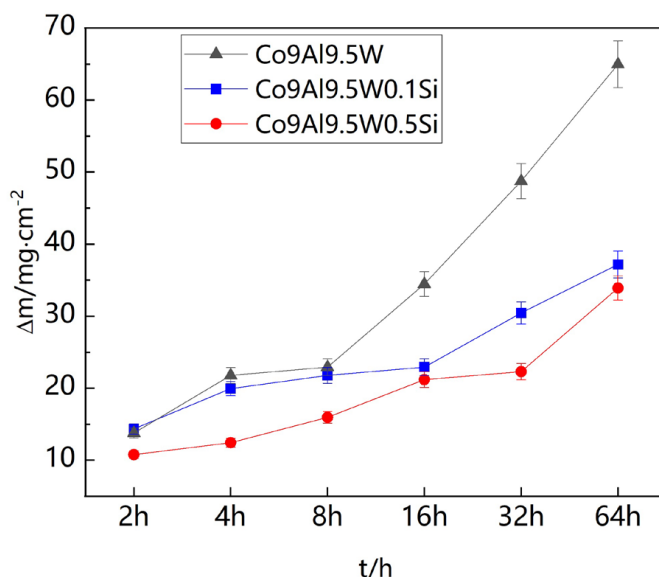


Figure 2. Corrosion kinetics of Co-Al-W-xSi-based superalloys in 75% Na_2SO_4 + 25% NaCl (wt.%) salts mixture at 900 °C.

A parabolic oxidation equation can be used to describe the hot corrosion process [29]

$$\left(\frac{\Delta m}{S}\right)^2 = k_P t + C \quad (1)$$

where $\frac{\Delta m}{S}$ is the specific mass gain (mass gain per unit area), k_P represents the parabolic constant, t is the holding time, and C is a constant. The rate constant of the Si-free alloy was $1.81 \times 10^{-8} \text{ g}^2 \text{cm}^{-4} \text{s}^{-1}$, but with the addition of minor contents of Si, the rate constant dropped to $4.95 \times 10^{-9} \text{ g}^2 \text{cm}^{-4} \text{s}^{-1}$ for the 0.1 Si alloy and $4.39 \times 10^{-9} \text{ g}^2 \text{cm}^{-4} \text{s}^{-1}$ for the 0.5 Si alloy. The oxidation rate constant of Co-5Al (wt.%, 10.7 in at.%) alloy was only between $3.3 \times 10^{-9} \text{ g}^2 \text{cm}^{-4} \text{s}^{-1}$ and $4.2 \times 10^{-9} \text{ g}^2 \text{cm}^{-4} \text{s}^{-1}$ at 900 °C [30]. The rate constant of Al71Co29 (at.%) alloy was $9.71 \times 10^{-12} \text{ g}^2 \text{cm}^{-4} \text{s}^{-1}$ for the first 15 h and $5.81 \times 10^{-12} \text{ g}^2 \text{cm}^{-4} \text{s}^{-1}$ for the second 15 h [29]. The Si-bearing alloy possessed a comparable oxidation rate with Co-5Al alloy but was much larger than that of the Al71Co29 alloy.

3.2. XRD Spectrum

Figure 3 reveals the XRD patterns of e alloys with varied Si content after hot corrosion for 2, 32, and 64 h at 900 °C. The corrosion products of alloys at these time intervals were similar, and the corrosion products mainly consisted of Co_3O_4 (PDF 43-1003), CoO (PDF 43-1004), Co_2AlO_4 (PDF38-0814), and CoWO_4 (PDF 15-0867) oxides. Only the type of corrosion products in the outer layer and the sub-outer layer can be detected by XRD, so no sulfide was identified in the XRD patterns. The outer corrosion products were primarily oxides.

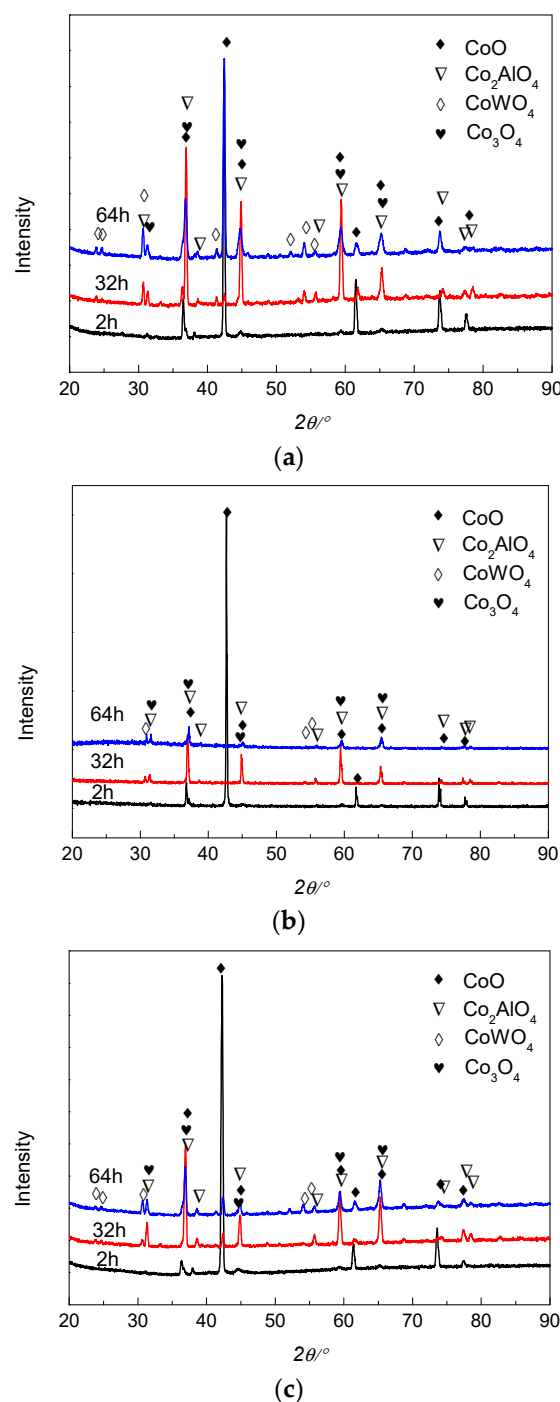


Figure 3. XRD spectrum of corrosion products obtained after hot corrosion in 75 wt.% Na_2SO_4 + 25 wt.% NaCl molten salts for (a) 2, (b) 32, (c) 64 h at 900 $^{\circ}\text{C}$.

3.3. Surface Morphologies

After corrosion, topographies of each sample for varied times are illustrated in Figures 4 and 5. Figure 4b shows that some micro-cracks on the surface of alloy A appeared after hot corrosion for 2 h. By contrast, the surface of the corrosion scales on alloys B and C was relatively even and compact, which can be seen in Figure 4d,f. The components indicated by arrow A in Figure 4a are mainly Co and O. The content of the Co element was 45.05% (at.%) and the content of the O element was 54.95%. Combined with the analysis of our XRD results, the adherent outer layers on the surface were a mixture of Co_3O_4 and CoO , while no sulfide was detected. According to the EDS energy

spectrum, the main components of the area indicated by arrow B in Figure 4d were Co and O, while the minor components were Na and W. The content of Co, O, Na, and W was 48.73%, 49.73%, 1.06%, and 0.48% respectively. The ratio of Co/O was greater than that of alloy A, which was close to the stoichiometric of CoO. This indicates that the primary component of the scale was CoO.

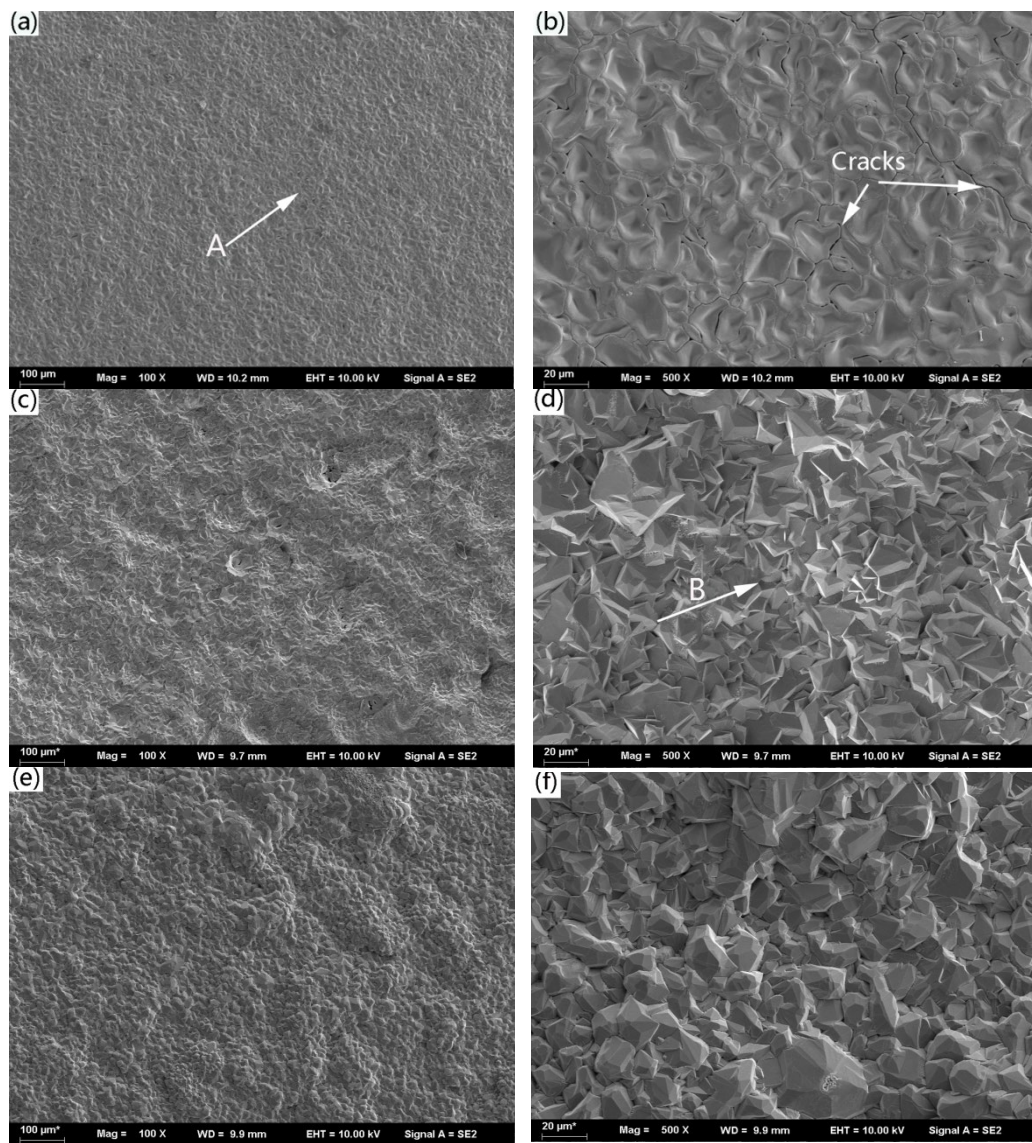


Figure 4. SEM surface morphologies of the alloys exposed to 25 wt.% NaCl + 75 wt.% Na₂SO₄ at 900 °C for varied times: (a,b) alloy A for 2 h; (c,d) alloy B for 2 h; (e,f) alloy C for 2 h.

Figure 5a–c,e demonstrate that after 32 h of hot corrosion of the three alloys, some scale spallation was present on the surface. This may have resulted from the thermal stress concentration between the corrosion scales, which destroyed its shape. The cracks could serve as diffusion channels of oxygen, to accelerate the corrosion process of the substrate. According to EDS analysis, the rod-like product indicated by arrow A in Figure 5b constituted mostly O and a small quantity of Co, W, and S. The content of O, Co, W, and S elements was 71.23%, 12.79%, 15.28%, and 0.7%, respectively, which indicates that the rod-like product was CoWO₄. The main components at the position indicated by arrow B were O and Co, as well as trace amounts of W. The content of the O element was 52.65%, and the content of the Co element was 46.42%. EDS measurements revealed that these products had compositions approaching the ideal composition of Co₃O₄ oxide. The rod-like

product indicated by arrow C in Figure 5d was CoWO_4 , which was similar to the CoWO_4 type oxide in Figure 5b.

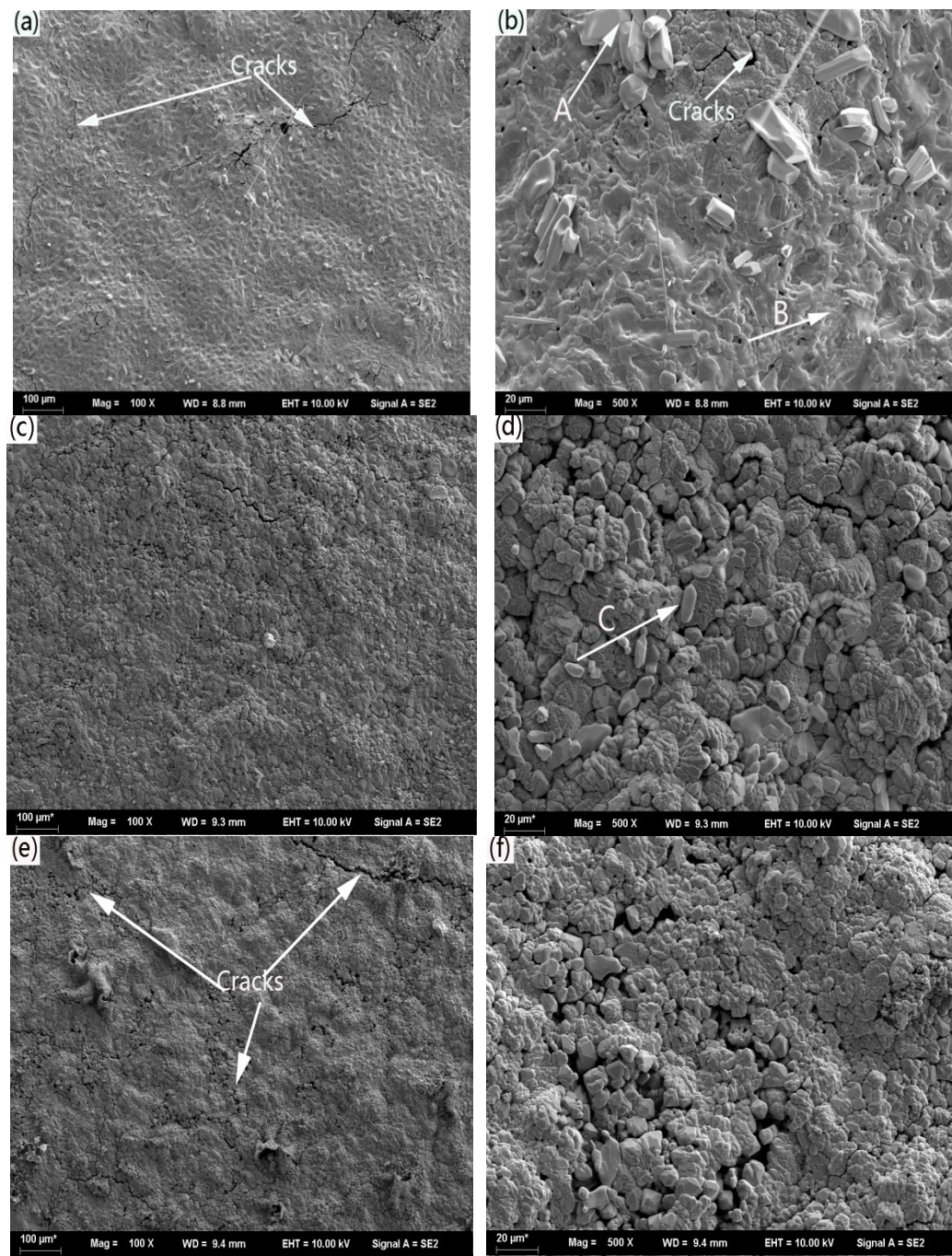


Figure 5. Topographies of the alloys exposed to 25 wt.% $\text{NaCl} + 75$ wt.% Na_2SO_4 at $900\text{ }^\circ\text{C}$ for different times: (a,b) alloy A for 32 h; (c,d) alloy B for 32 h; (e,f) alloy C for 32 h.

3.4. Cross-Section Morphologies

Figure 6 shows the cross-section morphologies of corrosion layers of the tested alloys after corrosion for 32 h. It illustrates that the thickness of the outer corrosion layer gradually decreased, and the density increased with the increment of Si content in the alloy. When this reached 0.5%, the outer corrosion layer became dense and continuous, so that it can inhibit the diffusion of O and S into the substrate and, thus, provided a better protective effect.

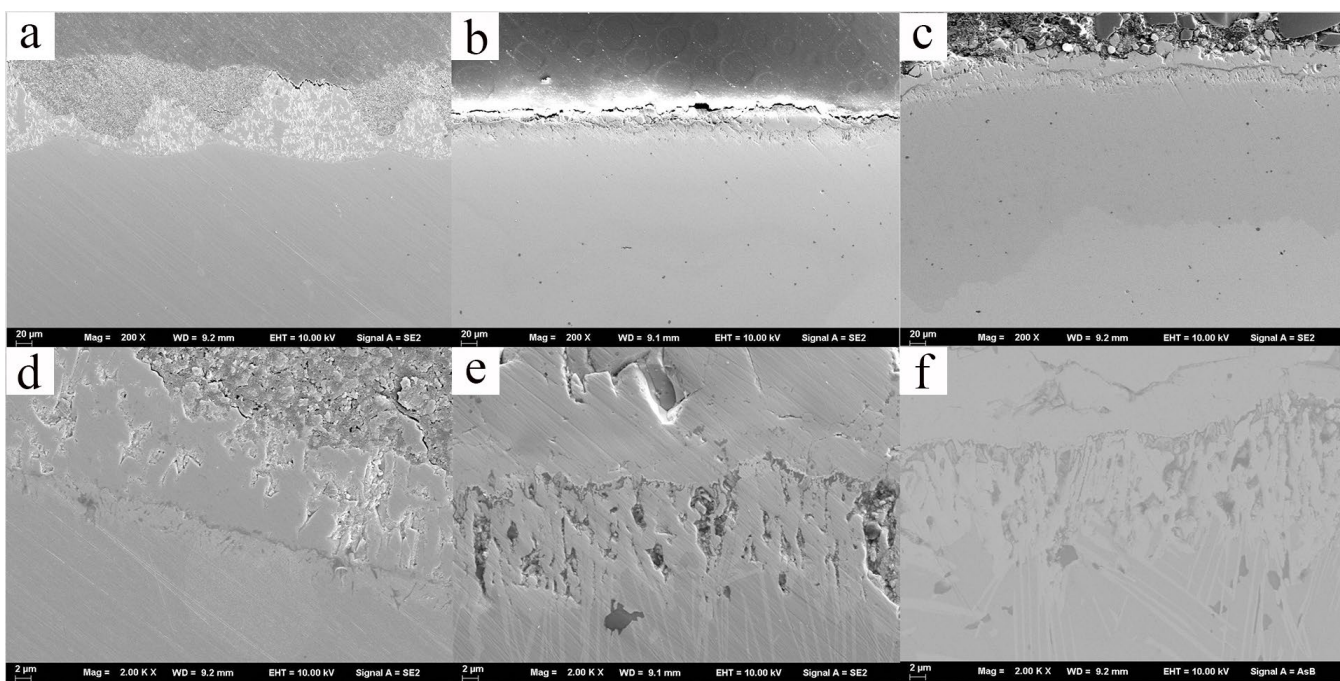


Figure 6. Cross-section SEM micrograph of the three alloys after exposure to the mixture of Na_2SO_4 and NaCl melts at $900\text{ }^\circ\text{C}$ for 32 h: (a) alloy A; (b) alloy B; (c) alloy C. Details of the Al-rich oxide layer and Co_3W layer (d–f).

Through comparison of the three samples, we observed that the oxidation layer of Si-free alloy was by far the thickest. As shown in Figure 6a,d, the alloy exhibited four different layers. The outer layer was a mixture of CoO and Co_3O_4 , which was porous. The second layer was a complex of CoWO_4 and CoAl_2O_4 , which was coarse and much more compact than the outer layer. The third layer was the Al-rich oxide layer. The inner layer was Co_3W , whose Al content was depleted. The details of the Al-rich oxide layer and Co_3W layer were revealed in Figure 6d–f.

The microphotographs and element mapping of the cross-section of the corrosion scale near the substrate of the three specimens are presented in Figure 7. Here, we observed that the intermediate transition layer was rich in Al, so a discontinuous layer of Al_2O_3 oxide film was developed in the base alloy. This can prevent the diffusion of O and S elements into the alloy. Depending on the oxidation temperature, whether the Al_2O_3 layer was continuous may be key to its protective role. Figure 7b shows that the Al-rich layer of Alloy A was thin and discrete and, thereby, it only played a limited role in protection. The layer of protective oxidation of Al_2O_3 was more significant in the 0.1 Si alloy than that of the Si-free alloy. The Al_2O_3 membrane can effectively prevent the diffusion of S and O into the substrate. The Al_2O_3 was relatively even and continuous, though still with some breakpoints. It can be observed from Figure 7h that the corrosion layer after the corrosion of C alloy for 32 h was separated into an outer and inner corrosion layer. The thickness of the outer corrosion layer was small, mainly rich in O, Si, and W elements, with a small part of the Co element. The intermediate layer was also a dense Al_2O_3 layer, which can help the alloy inhibit hot corrosion. In addition, from Figure 6c and d, we observed that the brighter part of the corrosion layer in the alloy contained primary O, Al, and W elements. This phase was stable at this temperature and was believed to reduce the detrimental effect of S, since the diffusion of S led to the reaction product of S and Al_2O_3 . The internal corrosion layer of the alloy mainly contained Co, W, and Si elements. Although no SiO_2 scale was observed in Figure 7, the Si showed an obvious outward diffusion trend and was rich in the oxide scale, outer layer, and intermediate layer, as seen in Figure 7g,k.

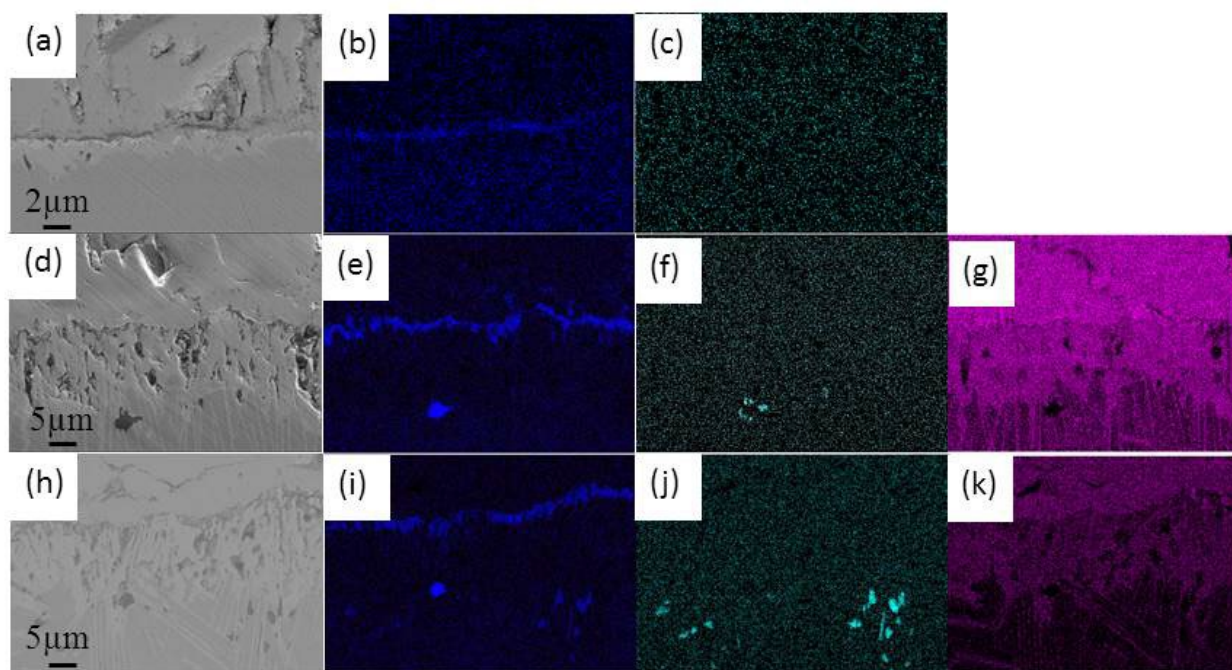


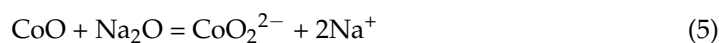
Figure 7. BSE micrographs of (a) Si-free (d) 0.1 Si (h) 0.5 Si alloys and EDS mappings Al, S and Si: Al (b,e,i); S (c,f,j), and Si (g,k) Alloys exposed to 25 wt.% NaCl + 75 wt.% Na₂SO₄ at 900 °C for 32 h.

4. Discussion

In the present study, new types of Co-based superalloys with added Si were designed and their hot corrosion behaviors were investigated at 900 °C. The present investigation showed that the molten Na₂SO₄ + NaCl-induced hot corrosion was severe and contained notably thick and porous scale forms. Hot corrosion can be viewed as accelerated oxidation in the presence of a mixture of molten Na₂SO₄ and NaCl [17,31]. During the hot corrosion experiment, oxidation emerged first because of the reaction between the O and the substrate [32]. Usage of the molten salts initiated a rapid failure of the protective oxide layer. Alumina was formed by selective oxidation, and mixed salts reacted easily with oxides. Under these conditions, it was difficult for the oxide to develop a continuous protective oxide layer, and consequently, hot corrosion occurred. The molten Na₂SO₄ decomposed into O₂ and S₂ at 900 °C, and two equilibria exist in the Na₂SO₄ [17].



The Na₂SO₄ can react with oxides formed under hot corrosion conditions. At the beginning stage of the hot corrosion, Co₃O₄, CoO, and Al₂O₃ formed due to the reaction between Co, Al, and O.



The ions produced (Al₂O₄²⁻, CoO₂²⁻, and Co₃O₅²⁻) may move from the molten salt/coating interface to the molten salt/air interface, where the basicity of the molten salt is low, and oxides can be reprecipitated by the decomposition of ions. This leads to the

reprecipitation of the porous oxides. The process repeats itself, and the porous scale of Co_3O_4 , CoO extends.



Johnson et al. examined the influence of NaCl and Na_2SO_4 on the high-temperature oxidation of Ni-based alloys [33]. The results demonstrate that Cl^- can advance the tendency of the scales to crack and spall during the initial oxidation. In the present study, NaCl in the mixed salts showed a similar impact [34–39].

Therefore, the presence of $\text{Na}_2\text{SO}_4 + \text{NaCl}$ molten salts leads to the formation of the porous scale on three alloys. Because of the standard Gibbs free energy changes for the metallic oxides and sulfides at 1173 K are listed in the order of $\text{Al}_2\text{O}_3 < \text{Cr}_2\text{O}_3 < \text{Al}_2\text{S}_3 < \text{CoO} < \text{CrS} < \text{NiO} < \text{Ni}_2\text{S}_3 < \text{Co}_9\text{S}_8$ [40,41], Al would react preferentially with O_2 penetrated through the scale to form Al_2O_3 . This brings about the precipitation of Al_2O_3 in the alloy (internal oxidation zone), which is stable and dense [42]. Furthermore, 0.2% Ce plays a similar role in a Co-Al-W alloy [43]. The addition of Si may play one of several roles in the resistance to hot corrosion: firstly, it eases the formation of a continuous dense Al_2O_3 ; secondly, Si diffuses outward, reducing cracks and spalling of the oxide scale, as illustrated in Figures 4 and 6.

5. Conclusions

The hot corrosion performance of a γ' precipitation-strengthened Co-Al-W-XSi (where Si = 0, 0.1, 0.5) were studied with the predeposition of $\text{Na}_2\text{SO}_4 + \text{NaCl}$ mixture at 900 °C. With the increase in Si content, the hot corrosion resistance of the alloy was substantially improved. The oxidation rate constant of Si-free alloy was $1.81 \times 10^{-8} \text{ g}^2\text{cm}^{-4}\text{s}^{-1}$, and when 0.5% Si was added into the alloy, the rate constant dropped to $4.39 \times 10^{-9} \text{ g}^2\text{cm}^{-4}\text{s}^{-1}$. The addition of Si promoted the formation of a continuous Al_2O_3 layer, which was beneficial for resistance to hot corrosion. In addition, the addition of Si may also reduce the intrusion of S and O by the formation of a stable oxide scale which is more resistant to crack and spallation.

Author Contributions: Conception, Y.Q. and S.C.; Materials preparation, Q.L.; Hot corrosion conduction, Y.W.; Analysis and writing, P.Z. All authors have read and agreed to the published version of the manuscript.

Funding: This research was funded by [National Natural Science Foundation of China], grant number [52275339] and [51471079].

Institutional Review Board Statement: Yanxin Qiao is an editorial board member for Coatings and was not involved in the editorial review or the decision to publish this article.

Informed Consent Statement: Not applicable.

Data Availability Statement: No extended data available.

Acknowledgments: We thank to Yigu Miao and William Bellamy for their language improvement.

Conflicts of Interest: The authors declare no conflict of interest.

References

1. Ma, L.N.; Wang, T.Y.; Zhang, Z. Influence of Short-time Oxidation on Corrosion Properties of Directionally Solidified Superalloys with Different Orientations. *J. Mater. Eng.* **2016**, *44*, 78–87.
2. Sung, J.K.; Hong, G.S.; Kim, W.Y.; Kim, M.S.; Chiba, A. Mechanical Property of Single Phase Co-Ni-Cr-Mo Based Superalloy Produced by Cold Working and Recrystallization Heat Treatment. *Mater. Sci. Forum.* **2004**, *449–452*, 573–576. [[CrossRef](#)]
3. Klein, L.; Killian, M.S.; Virtanen, S. The effect of nickel and silicon addition on some oxidation properties of novel Co-based high temperature alloys. *Corros. Sci.* **2013**, *69*, 43–49. [[CrossRef](#)]

4. Yang, L.; Bo, C.; Junwei, W.; Zhiping, W.; Wensheng, L. Corrosion Behavior of Cr, Fe and Ni Based Superalloy in Molten NaCl. *Rare Metal. Mat. Eng.* **2014**, *43*, 17–23. [[CrossRef](#)]
5. Hongfang, M.; Ming, Z.; Yunmiao, Z. Corrosion behavior of two kinds of alloys in chloride molten salts. *Mater. Rev.* **2014**, *28*, 109–113.
6. Huang, Q.Y.; Li, H.K. *High Temperature Alloy*; Metallurgical Industry Press: Beijing, China, 2000; pp. 100–133.
7. Zhu, R.; Guo, M.J.; Zuo, Y. A study of the mechanism of internal sulfidation-internal oxidation during hot corrosion of Ni-base alloys. *Oxid. Met.* **1987**, *27*, 253–265.
8. Kameswa, S.R. The role of NaCl in the hot-corrosion behavior of nimonicalloy 90. *Oxid. Met.* **1986**, *26*, 33–44. [[CrossRef](#)]
9. Cui, H.; Zhang, J.; Murata, Y. Hot corrosion behavior of Ni-based superalloys with higher Cr contents—Part II. mechanism of hot corrosion behavior. *J. Univ. Sci. Technol. B* **1996**, *3*, 91.
10. Klein, L.; Virtanen, S. Corrosion properties of novel γ' -strengthened Co-base superalloys. *Corros. Sci.* **2013**, *66*, 233–241. [[CrossRef](#)]
11. Lass, E.A.; Williams, M.E.; Campbell, C.E.; Moon, K.W.; Kattner, U.R. γ' Phase Stability and Phase Equilibrium in Ternary Co-Al-W at 900 °C. *J. Phase Equilib. Diff.* **2014**, *35*, 711–723. [[CrossRef](#)]
12. Akane, S.; Pollock, T.M. High-temperature strength and deformation of γ/γ' two-phase Co-Al-W-base alloys. *Acta Mater.* **2008**, *56*, 1288–1297.
13. Sato, J.; Tomori, T.; Oikawa, K. Cobalt-base high-temperature alloys. *Science* **2006**, *90*, 312. [[CrossRef](#)] [[PubMed](#)]
14. Kazuya, S.; Toshihiro, O.; Jun, S.; Katsunari, O.; Ikuo, O.; Ryosuke, K.; Kiyohito, I. Phase equilibria and microstructure on γ' phase in Co-Ni-Al-W system. *Mater. Trans.* **2008**, *49*, 1474–1479.
15. Yang, S.Y.; Jiang, M.; Wang, L. Thermodynamic analysis of γ and γ' phases in new-type co-based superalloy. *J. Northeast. Univ.* **2012**, *33*, 1274–1277.
16. Young, D.J. *High Temperature Oxidation and Corrosion of Metals*; Elsevier: Amsterdam, The Netherlands, 2008.
17. Goebel, J.A.; Pettit, F.S.; Goward, G.W. Mechanisms for the hot corrosion of nickel-base alloys. *Metall. Trans.* **1973**, *4*, 261–278. [[CrossRef](#)]
18. Yan, H.Y.; Vorontsov, V.A.; Dye, D. Effect of alloying on the oxidation behaviour of Co-Al-W superalloys. *Corros. Sci.* **2014**, *83*, 382–395. [[CrossRef](#)]
19. Lu, J.; Zhu, S.; Wang, F. High temperature corrosion behavior of an AIP NiCoCrAlY coating modified by aluminizing. *Surf. Coat. Technol.* **2011**, *205*, 5053. [[CrossRef](#)]
20. Jiang, S.M.; Peng, X.; Bao, Z.B.; Liu, S.C.; Wang, Q.M.; Gong, J.; Sun, C. Preparation and hot corrosion behaviour of a MCrAlY + AlSiY composite coating. *Corros. Sci.* **2008**, *50*, 3213. [[CrossRef](#)]
21. Huang, D.; Qiao, Y.X.; Yang, L.L.; Wang, J.L.; Chen, M.H.; Zhu, S.L.; Wang, F.H. Effect of shot peening of substrate surface on cyclic oxidation behavior of sputtered nanocrystalline coating. *Acta Metall. Sin.* **2023**, *59*, 668–678.
22. Suzuki, A.; Wu, F.; Murakami, H.; Imai, H. High temperature characteristics of Ir-Ta coated and aluminized Ni-base single crystal superalloys. *Sci. Technol. Adv. Mater.* **2004**, *5*, 555. [[CrossRef](#)]
23. Wang, J.; Zhou, L.; Sheng, L.; Guo, J. The microstructure evolution and its effect on the mechanical properties of a hotcorrosion resistant Ni-based superalloy during long-term thermal exposure. *Mater. Des.* **2012**, *39*, 55. [[CrossRef](#)]
24. Yan, H.Y.; Vorontsov, V.A.; Dye, D. Alloying effects in polycrystalline γ' , strengthened Co-Al-W base alloys. *Intermetallics* **2014**, *48*, 44–53. [[CrossRef](#)]
25. Jiang, S.M.; Li, H.Q.; Ma, J.; Xu, C.; Gong, J.; Sun, C. High temperature corrosion behaviour of a gradient NiCoCrAlYSi coating II: Oxidation and hot corrosion. *Corros. Sci.* **2010**, *52*, 2316–2322. [[CrossRef](#)]
26. Gao, B.; Wang, L.; Liu, Y.; Song, X.; Yang, S.-Y.; Yao, Z.-Y. Corrosion behavior of new type Co-based superalloys with different Ni contents. *Corros. Rev.* **2017**, *35*, 455–462. [[CrossRef](#)]
27. Xu, Y.T.; Xia, T.D.; Yan, J.Q. Effect of alloying elements to hot corrosion behavior of novel Co-Al-W superalloy. *J. Chin. Soc. Corros. Protect.* **2010**, *30*, 457–464.
28. Klein, L.; Bauer, A.; Neumeier, S.; Göken, M.; Virtanen, S. High temperature oxidation of γ/γ' -strengthened Co-base superalloys. *Corros. Sci.* **2011**, *53*, 2027–2034. [[CrossRef](#)]
29. Šulhánek, P.; Drienovský, M.; Černičková, I.; Ďuriška, L.; Skaudžius, R.; Gerhátová, Ž.; Palcut, M. Oxidation of Al-Co Alloys at High Temperatures. *Materials* **2020**, *13*, 3152. [[CrossRef](#)] [[PubMed](#)]
30. Irving, G.N.; Stringer, J.; Whittle, D.P. The high-temperature oxidation resistance of Co-Al alloys. *Oxid. Met.* **1975**, *9*, 427–440. [[CrossRef](#)]
31. Eliaz, N.; Shemesh, G.; Latanision, R.M. Hot corrosion in gas turbine components. *Eng. Fail. Anal.* **2002**, *9*, 31–43. [[CrossRef](#)]
32. Li, Y.Z.; Pyczak, F.; Paulb, J.; Yaoa, Z. Oxidation behaviors of Co-Al-W-0.1B superalloys in a long-term isothermal exposure at 900 °C. *J. Mater. Sci. Technol.* **2018**, *34*, 2212–2217. [[CrossRef](#)]
33. Johnson, J.B.; Nicholls, J.R.; Hurst, R.C.; Hancock, P. The mechanical properties of surface scales on nickel-base superalloys-II. Contaminant corrosion. *Corros. Sci.* **1978**, *18*, 543. [[CrossRef](#)]
34. Sreedhara, G.; Raja, V.S. Hot corrosion of YSZ/Al₂O₃ dispersed NiCrAlYplasmasprayed coatings in Na₂SO₄–10 wt.%NaCl Melt. *Corros. Sci.* **2010**, *52*, 2592–2602. [[CrossRef](#)]
35. Young, D.J.; Gleeson, B. Alloy phase transformations driven by high temperature corrosion processes. *Corros. Sci.* **2002**, *44*, 345–357. [[CrossRef](#)]
36. Shinata, Y.; Nishi, Y. NaCl-induced accelerated oxidation of chromium. *Oxid. Met.* **1986**, *26*, 201–212. [[CrossRef](#)]

37. Yao, Z.; Marek, M. NaCl-induced hot corrosion of a titanium aluminide alloy. *Mater. Sci. Eng. A* **1995**, *192*, 994–1000. [[CrossRef](#)]
38. Li, Y.S. *High Temperature Oxidation and Chlorination of Metal Materials*; Dalian Institute of Science and Technology Press: Dalian, China, 2001.
39. McKee, D.W.; Shore, D.A.; Lurthra, K.L. The effect of SO₂ and NaCl on high temperature hot corrosion. *J. Electrochem. Soc.* **1978**, *125*, 411–419. [[CrossRef](#)]
40. Ye, D.L.; Hu, J.H. *Practical Inorganic Thermodynamic Data Manual Microtrainedinflux*; Metallurgical Industry Press: Beijing, China, 2002.
41. Barin, I. *Thermochemical Data of Pure Substances*; Science Press: Beijing, China, 2003; Volume 2.
42. Forsik, S.A.J.; Rosas, A.O.P.; Wang, T.; Colombo, G.A.; Zhou, N.; Kernion, S.J.; Epler, M.E. High-Temperature Oxidation Behavior of a Novel Co-Base Superalloy. *Metall. Mater. Trans. A* **2018**, *49A*, 4058–4069. [[CrossRef](#)]
43. Guan, Q.; Zhong, F.; Sha, J. Effect of Ce addition on hot corrosion behaviours of a cast γ'-strengthened Co-Al-W-Mo-Ta-B alloy at 800 °C. *Prog. Nat. Sci.-Mater.* **2022**, *32*, 463–471. [[CrossRef](#)]

Disclaimer/Publisher's Note: The statements, opinions and data contained in all publications are solely those of the individual author(s) and contributor(s) and not of MDPI and/or the editor(s). MDPI and/or the editor(s) disclaim responsibility for any injury to people or property resulting from any ideas, methods, instructions or products referred to in the content.